Atom probe tomography quantification of carbon in silicon

P. Dumas, Sébastien Duguay, J. Borrel, F. Hilario, Didier Blavette

Atom probe tomography quantification of carbon in silicon

P.Dumas [1,2] ; S.Duguay [2] ; J.Borrel [1] ; F.Hilario [1] ; D.Blavette [2]

[1] STMicroelectronics Crolles, France
[2] Université de Rouen, GPM, UMR CNRS 6634, France

Abstract

Atom Probe Tomography (APT) was used to quantify carbon in implanted silicon at two various electric fields (~ 15 and 20 V/nm). Using equal proportions of implanted ^{12}C and ^{13}C, the numerous molecular ions that were observed were identified and their contribution to the carbon content statistically derived. Much more accurate carbon quantification was obtained in the lowest electric field analysis by comparing APT with Secondary Ion Mass Spectroscopy profiles. This was assigned to a lower amount of molecular ion dissociations. Furthermore, the number of self-interstitials trapped per carbon atom in clusters was derived. This value of interest for the microelectronics industry regarding dopant diffusion and implantation induced defects was estimated close to one, in agreement with the expected stoichiometry of the SiC phase present in the phase diagram. However, this was obtained only when using low electric field conditions.

1. Introduction

Quantification of carbon in materials using Atom Probe Tomography (APT) is a tricky issue. Large underestimation in the carbon content is indeed observed [1,2,3].

One well known reason of carbon biases arises from the occurrence of multiple events and related detection biases. This occurs when several ions strike the detector nearly simultaneously and close to each other [3]. When this happens, a part of ions may be lost due to the so-called electronic “dead time” and “dead zone” existing between each hit [3,5,6]. This phenomenon is very likely when analyzing carbon because the high electric field needed to induce its evaporation promotes correlated departures of carbon ions at the tip surface [1,3]. Another source of carbon multi-events is the dissociation of molecular ions during their flight from the tip to the detector [4,7].

An additional complication comes from the detection of carbon ions sharing the same mass-to-charge ratio, like $(C_2)^{2+}$ and C^+. When this happens, the proportion of each overlapped ion is needed to make a correct quantification. In some cases, it is possible to derive theses proportions from isotopes abundance [1,9,10]. However, in the field of ion implantation, only one isotope is selected though the mass analyzer. As ^{12}C accounts for 98.93 % of the natural isotopic repartition, $^{12}C^+$ ions are usually selected to minimize the process time. As a result, mass-to-charge ratio overlaps cannot be solved using the isotope proportion method. For materials featuring the natural repartition of carbon (metallic alloys and other

semiconductors), peak overlaps of minor species can still be solved at the expense of a higher level of uncertainty [8]. This uncertainty is lower if both ^{12}C and ^{13}C isotopes are present in similar proportions.

In this study, the issue faced using isotope abundance to solve carbon overlaps in low concentrated silicon will be overcome by implanting $^{12}C^+$ and $^{13}C^+$ in equal proportion. A statistical approach will be used to identify the molecular ions and quantify their contribution to the implanted concentration at two electric fields. The ambition is to clarify the contribution of various bias sources in overall biases. Although this study has been carried in carbon implanted silicon, results and conclusions may be transposed to carbon quantification in general.

Another aim of this work is to study carbon clustering. In the microelectronics industry, carbon is co-implanted in silicon to suppress transient enhanced diffusion of interstitially mediated dopants (boron and phosphorus) and the formation of extended defects [11,16,17]. Carbon is indeed known to consume self-interstitials, notably through the formation of clusters. The number of self-interstitials trapped per carbon atom in clusters, or in other words the atomic fraction of carbon in clusters, will be here measured using APT.

2. Materials and method

$^{12}C^+$ and $^{13}C^+$ ion implantations were performed at room temperature in a (100) oriented 300 mm silicon wafer. Doses, energies and tilts used were $1 \pm 0.01 \times 10^{15}$ ions cm^{-2}, 30 keV and 3° respectively in the objective to get both ^{12}C and ^{13}C profiles very close to each other and centered around 100 nm in depth with a maximum carbon content of 0.2 at. %. Because increasing the number of implantation cycles is thought to lead to a better superimposition between ^{12}C and ^{13}C profiles, the total dose D ($2 \pm 0.02 \times 10^{15}$ ions cm^{-2}) was implanted in 4 cycles, each cycle composed of one $^{12}C^+$ sub-implant at D/8 followed by one $^{13}C^+$ sub-implant at D/8. The wafer was then annealed at an average temperature of 750 °C for 5 h. Details of the annealing sequence applied are found in [11]. In addition to restoring silicon crystallinity, this sequence is known to induce carbon clustering. Afterwards, carbon concentration profile was obtained from a CAMECA IMS dynamic Secondary Ion Mass Spectroscopy (SIMS) using a cesium beam at 4 keV, a beam current of 100 nA , and a sputtering rate of 0.41 nm/s. SIMS quantification was assessed from ion implantation doses.

A 1 cm^2 sample was then cut-off from the annealed wafer for APT tip preparation. Using a G4 CXe Dualbeam plasma focused ion beam, a small volume of annealed silicon was lifted-out and attached to a tungsten needle. Two sharp tips of around 30 nm diameter were then obtained from this volume using ion beam milling (see Fig. 1). Such small diameters are needed to generate the high electric field (~20 V/nm) that is required in APT analyses. These latter were conducted using a Laser-Assisted-Wide-Angle Tomographic Atom Probe (CAMECA-LAWATAP). The laser was operated at a 343 nm wavelength under ultra-vacuum conditions ($\sim 10^{-10}$ Torr) at a 100 kHz repetition rate and was focused on a 0.1 mm spot diameter. The tip

temperature was maintained at 80 K. After preparation and APT analyses, Xe is found to be below detection limits of APT.

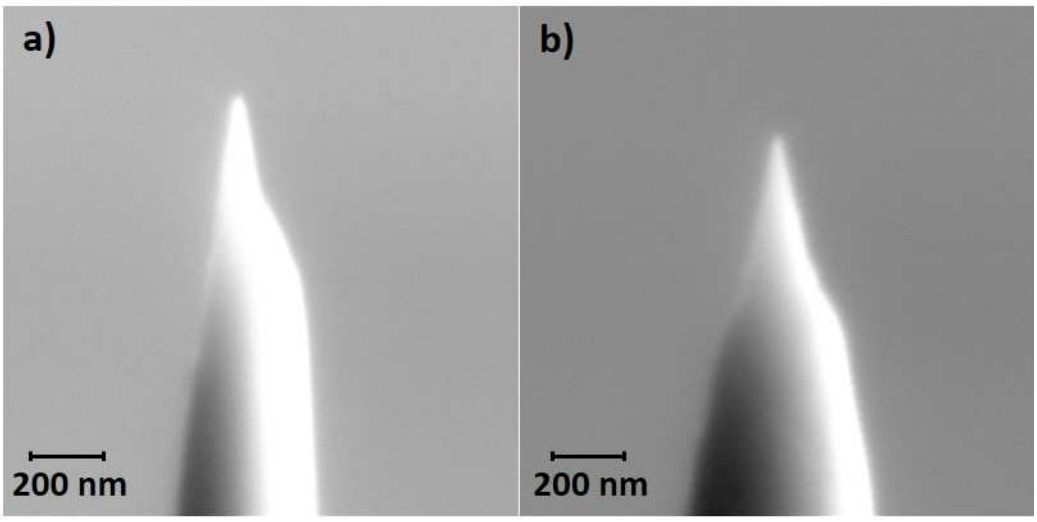

Fig. 1. Scanning electron microscopy images of the tips before APT analysis a) tip analyzed at the highest electric field (tip diameter : 38 +/- 3 nm) b) tip analyzed at the lowest electric field (tip diameter : 28 +/- 3 nm).

3. Results and discussion

APT analyses were conducted using two laser powers *(10 and 80 nJ/pulse)* to elucidate the influence of the evaporation field on carbon quantification. The two mass spectra plotted in Fig. 2 represent the normalized number of detected ions as a function of the mass-to-charge ratio, at a given laser power. Kingham curves and Si^{+}/Si^{2+}ratio were used to assess electric fields at the tip surface [12]. They were found to be close to 15 and 20 V/nm and will be denoted hereinafter respectively as the lowest (and highest) electric field analysis.

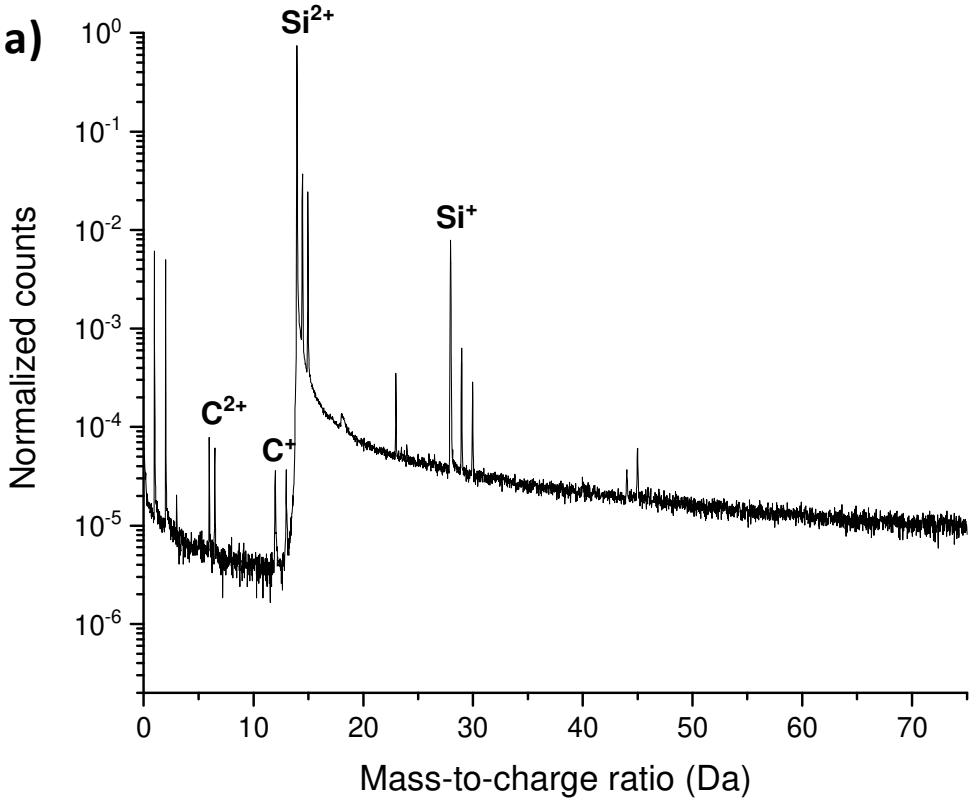
a)
Si2+
Si+
C2+
C+
Normalized counts
Mass-to-charge ratio (Da)

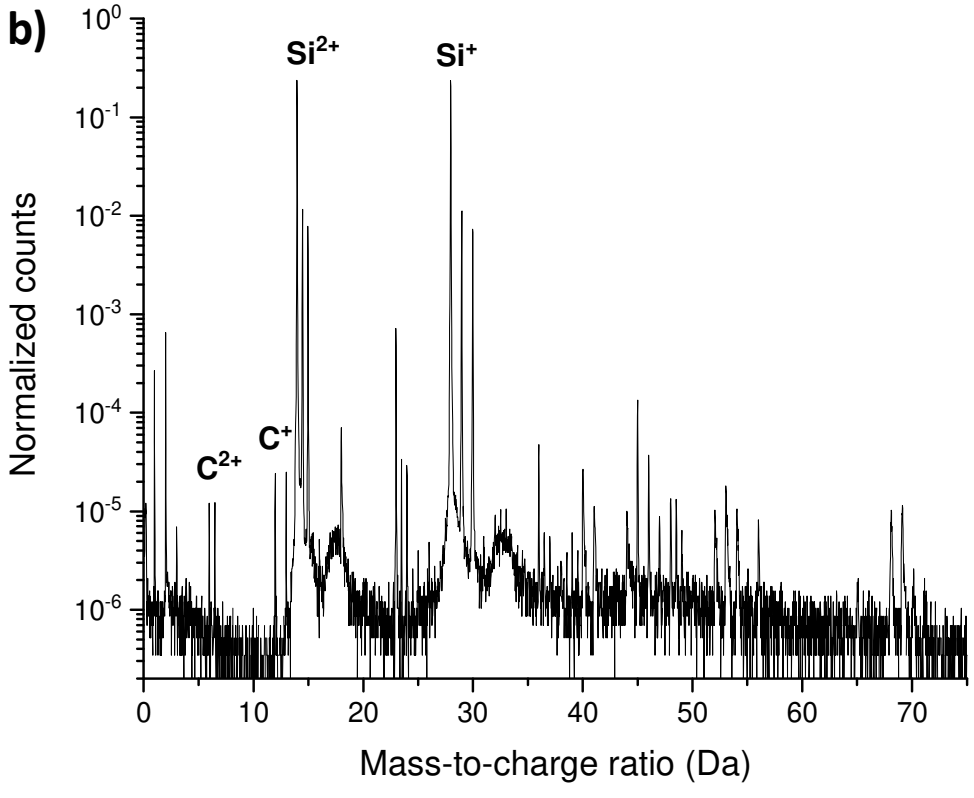
b)
Si2+
Si+
C2+
C+
Normalized counts
Mass-to-charge ratio (Da)

Fig .2. Mass spectra related to the analysis of C implanted silicon samples a) highest electric field analysis (10.160 million atoms and Si^+/Si^{2+}= 0.02) b) lowest electric field analysis (6.089 million atoms and Si^+/Si^{2+} = 1.7). Counts are normalized to the total number of atoms in each analyzed volume.

First, aside the expected presence of monoatomic C^+ and C^{2+} ions from 6 to 13 Da (Fig. 2 a) b)), numerous other peaks were detected from 20 to 75 Da in the lowest electric field analysis (Fig. 2 b)). The latter are likely to be related to molecular ions evaporated from carbon-enriched clusters that nucleate due to carbon supersaturation. The carbon solubility limit in silicon, around 2 ppb at 750°C [18], is indeed very low compared to the carbon amount. The same range of peaks is not visible in Fig. 2 a) as it is hidden by the tails of $^{28}Si^+$ and $^{28}Si^{2+}$ peaks. These so-called thermal tails are related to $^{28}Si^+$ and $^{28}Si^{2+}$ ions evaporated after laser pulses during the cooling of the tip [13,14]. This phenomenon is enhanced when using higher electric fields [15] (i.e. lower laser powers at a given evaporation rate) as highlighted in Fig. 2 a).

A cluster identification was applied to the lowest electric field using the iso-position method [20]. The purpose of this identification was not quantitative but to build a mass spectrum less noisy than that in Fig. 2 b), to make the peaks related to molecular ions more distinct and their identification easier. The objective is to exclude from the analysis silicon atoms that are not present in peaks related to molecular ions (from 20 to 75 Da). To optimize the signal/noise ratio in the cluster identification process, only the well-defined peaks related to $^{12}C^{+/2+}$ and $^{13}C^{+/2+}$ were considered. The concentration threshold was taken to 0.05% and the minimal number of atoms per cluster to 5. Once again, these parameters do not necessarily account for the real size or the volume fraction of the clusters but were chosen to build a less noisy mass spectrum (Fig. 3). For identification purpose, detected ions were classified by families labelled as $(Si_nC_p)^{q+}$ where *n* and *p* respectively represent the number of silicon and carbon atoms, and *q* is the ion charge number (Fig. 3). For instance, the C^+ family comprises $^{12}C^+$ and $^{13}C^+$ ions. Applying the same cluster identification to data related to the highest electric field analysis allowed to identify molecular ions which were previously hidden by the Si^+ and Si^{2+} tails. However, only 4 molecular families involving carbon were detected : $(C(H_20)_2)^{2+}$, $(C_2)^+$, $(SiC_2)^+$ and $(SiC)^+$ against 13 in the lowest electric field analysis.

For a given $(Si_nC_p)^{q+}$ family, we define its multiplicity as the number of different ways to form $(Si_nC_p)^{q+}$ ions from silicon and carbon isotopes. For example, for *n*=0, the multiplicity of the $(C_2)^+$ family is three as it is composed of $(^{12}C^{12}C)^+$, $(^{13}C^{13}C)^+$ and $(^{12}C^{13}C)^+$ ions. A general formula is derived as follows. Let us first consider a family composed of *k* identical elements having *z* isotopes. Its multiplicity, also called multiset coefficient in combinatorics [21], is equal to $\binom{z+k-1}{k}$ which denotes the number of combinations of *k* out of *z + k – 1*. For a given $(Si_nC_p)^{q+}$ family, its multiplicity labelled γ(n,p) is then the product of γ(n,0) and γ(0,p):

$$\gamma(n,p) = \binom{3+n-1}{n}\binom{2+p-1}{p} = \frac{(n+1)(n+2)(p+1)}{2} \quad (1)$$

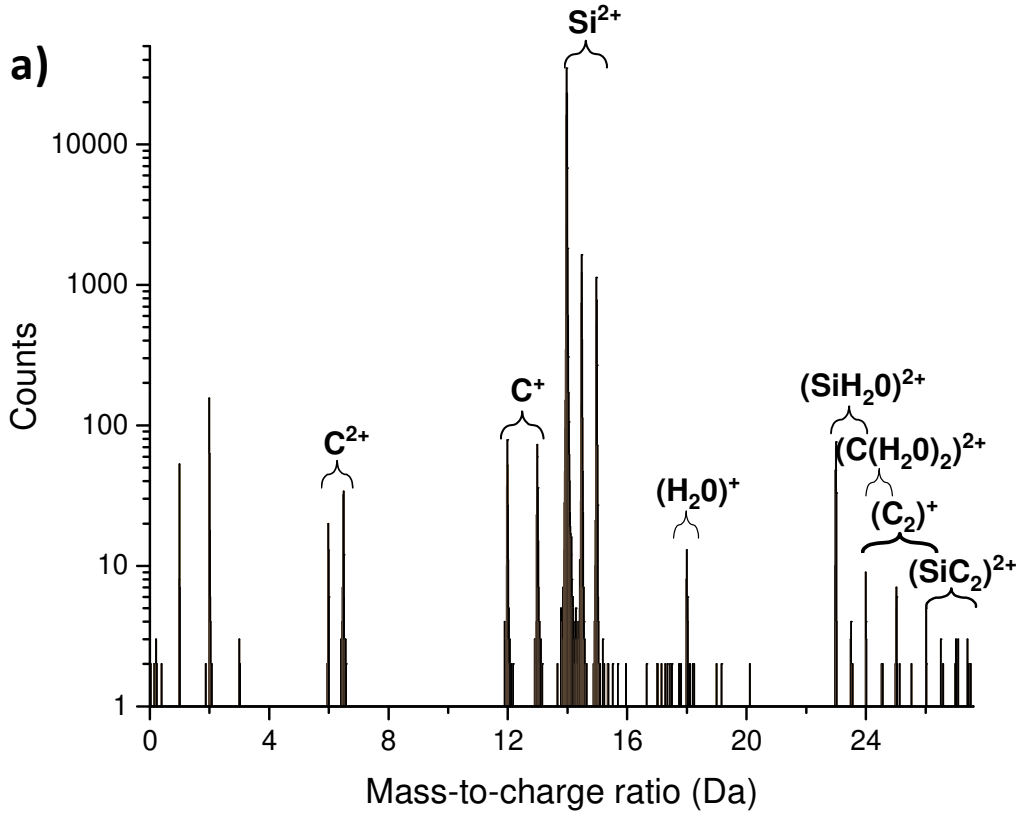
a)
Counts
10000
1000
100
10
1
0
4
8
12
16
20
24
Mass-to-charge ratio (Da)
Si^{2+}
C^{2+}
C^{+}
$(H_20)^{+}$
$(SiH_20)^{2+}$
$(C(H_20)_2)^{2+}$
$(C_2)^{+}$
$(SiC_2)^{2+}$

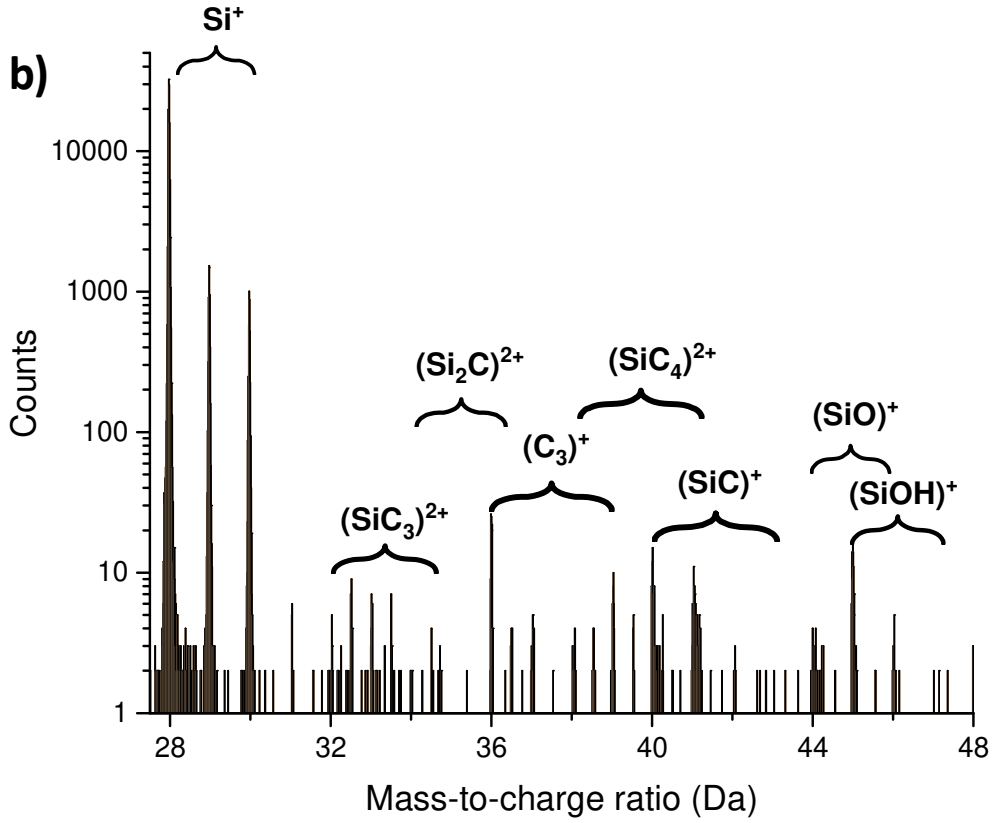
b)
Counts
10000
1000
100
10
1
28
32
36
40
44
48
Mass-to-charge ratio (Da)
Si^{+}
$(Si_2C)^{2+}$
$(SiC_4)^{2+}$
$(SiO)^{+}$
$(C_3)^{+}$
$(SiC)^{+}$
$(SiC_3)^{2+}$
$(SiOH)^{+}$

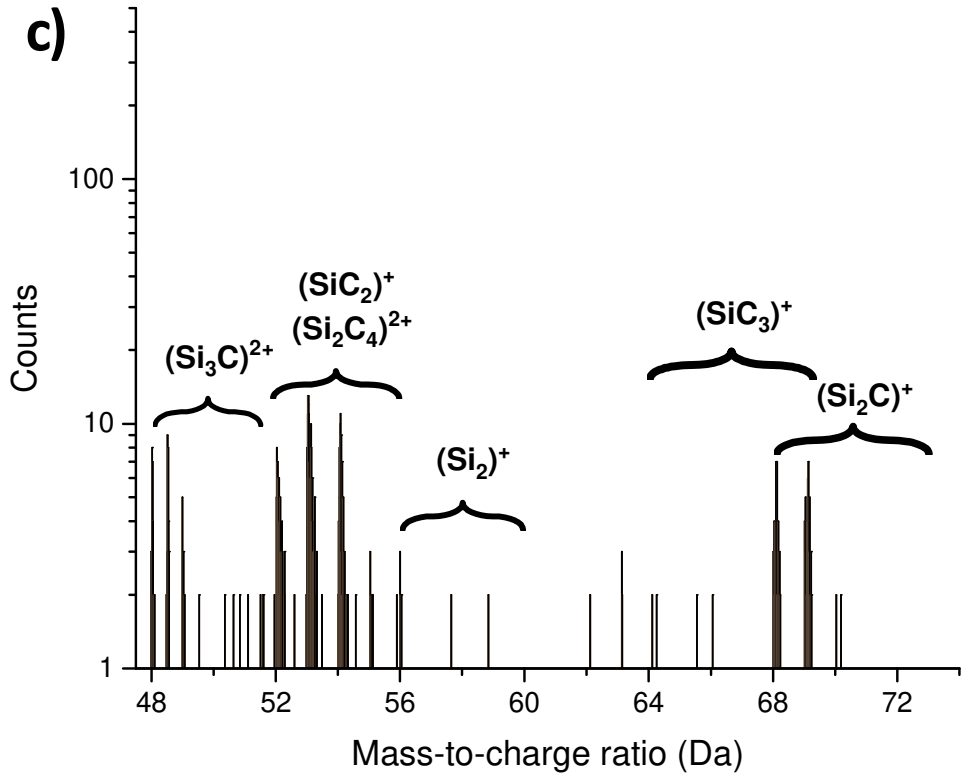

Fig .3. Mass spectra related to the filtered ions from the cluster identification (lowest electric field analysis). Peaks are identified by family in the range a) 0 to 28 Da b) 28 to 48 Da c) 48 to 74 Da.

The multiplicity of pure molecular ions composed of *p* carbon ions is simply equal to *p + 1*. Equation (1) is helpful to avoid missing contributions in peak identification, especially for large mixed families. It is worth mentioning that the observed number of peaks relative to a family is always lower or equal to its multiplicity. This is due to overlaps between peaks of the considered family that have the same mass-to-charge ratio. For instance, the number of peaks relative to the $(SiC)^+$ family is equal to 4 (at 40, 41, 42 and 43 Da) whereas γ(1,1) = 6 from equation (1). There are indeed 6 different types of ions belonging to the $(SiC)^+$ family but four of them share the same mass-to-charge ratio at 41 and 42 Da (see Table 1).

m/q (Da)	40	41	42	43
$(SiC)^+$ family	$(^{28}Si^{12}C)^+$	$(^{28}Si^{13}C)^+$ $(^{29}Si^{12}C)^+$	$(^{29}Si^{13}C)^+$ $(^{30}Si^{12}C)^+$	$(^{30}Si^{13}C)^+$
Proportion of counts (%)	46.11	46.11 2.345	2.345 1.545	1.545

Table 1 : Ions belonging to the $(SiC)^+$ family and their respective proportion of counts (lowest electric field analysis).

When there is an overlap, each contribution at the considered peak can be statistically derived from isotopic proportions. For this purpose, we define $f(n_{28},n_{29},n_{30},p_{12})$ as the proportion of counts of a given type of ion composed of n_{28} ^{28}Si, n_{29} ^{29}Si, n_{30} ^{30}Si , p_{12} ^{12}C and $(p - p_{12})$ ^{13}C relative to its family $(Si_nC_p)^{q+}$. This latter is derived from isotopic natural abundances and combinations:

$$f(n_{28},n_{29},n_{30},p_{12}) = \frac{1}{2^p}\binom{p}{p_{12}}\binom{n}{n_{28}}\binom{n-n_{28}}{n_{29}} {z_{28}}^{n_{28}}{z_{29}}^{n_{29}}{z_{30}}^{n_{30}} \quad (2)$$

Where z_{28}, z_{29} and z_{30} are the natural proportions of silicon isotopes taken to 92.22%, 4.69%, and 3.09%, respectively. Proportions of carbon isotopes were obtained by comparing ^{12}C and ^{13}C SIMS profiles (Fig. 5). Centered around 100 nm, profiles have nearly gaussian shapes which are typical of ion implantation. Additional peaks around 60 and 75 nm are likely to reveal carbon segregations to extended defects, like those detected in [11]. Furthermore, an ^{12}C accumulation is observed from the surface to 25 nm. This is attributed to an atmospheric contamination. ^{13}C contamination being around 100 times smaller than that of ^{12}C from isotopic natural proportions, it is screened by ^{13}C implanted concentration. Despite the difference at the surface, ^{12}C and ^{13}C SIMS profiles are practically superimposed all over the implantation axis. The fact that ^{12}C and ^{13}C are in equal proportions is expressed in equation (2) by the $\frac{1}{2^p}$ term. A numerical application is given in Table 1. It shows that the repartition of the $(SiC)^+$ family is mainly governed by ions containing ^{28}Si, the most abundant silicon isotope. Note that in this example, proportions were simply obtained by dividing natural proportions of silicon isotopes by 2, as ^{12}C and ^{13}C are in equal proportions.

Examples of overlaps resolution between ions from different families are given in the following. $(^{13}C^{13}C)^+$ and $(^{28}Si^{12}C^{12}C)^{2+}$ ions were detected at 26 Da. $(^{13}C^{13}C)^+$ counts are half $(^{12}C^{13}C)^+$ counts in agreement with equation (2). Because there is no overlap at 25 Da, $(^{13}C^{13}C)^+$ counts are also half 25 Da counts. $(^{28}Si\,^{12}C^{12}C)^{2+}$ counts were then obtained from the difference between 26 Da and $(^{13}C^{13}C)^+$ counts. *For each peak, background counts were accounted locally by defining another element of the same mass window in the close vicinity of the considered peak [10]*. Background counts were then subtracted to obtain the true number of counts relative to each ion. Due to ^{13}C low natural abundance (1.07%), no peak is usually detected at 12.5 Da leaving the overlap between $(C_2)^{2+}$ and C^+ ions unsolved. However, because ^{12}C and ^{13}C are here in equal proportions, $(^{12}C^{13}C)^{2+}$ ions accounts for 50% of the overall counts of $(C_2)^{2+}$ family. As there is no peak at 12.5 Da in both mass spectrum, we conclude that $(C_2)^{2+}$ ions are absent or below the detection limit in our experimental conditions.

$(C_3)^+$ ions have also been detected at 36, 37, 38 and 39 Da (Fig. 2 b)). Peak at 36 Da is the most pronounced among $(C_3)^+$ peaks whereas the proportion of $(^{12}C^{12}C^{12}C)^+$ ions should be equal to $(^{13}C^{13}C^{13}C)^+$ relative to $(C_3)^+$. This highlights the presence of another type of ions at 36 Da that we have interpreted as $((H_2O)_2)^+$. The relative importance of $(C_3)^+$ family in the overall carbon content can still be deduced, for example from the peak at 38 Da.

Complete carbon quantification was done through decorrelations of various overlapped ions. Families respective contributions to the carbon content were sorted in mass-to-charge ratio increasing order and plotted in a histogram (Fig. 4). The highest (respectively lowest) electric field analysis contributions are concentrated to the left (respectively right) hand side of the histogram. This trend indicates that the contribution of molecular ions is well lower in the highest electric field analysis (45% against 90%). We believe that this difference is attributed to the promotion of molecular ion dissociations at higher electric fields [3,7]. This would explain why molecular families at high mass-to-charge ratios (> 40 Da) were not detected in the highest electric field analysis. Note that the above assumption is difficult to prove in our experimental conditions. First, no dissociation tracks were observed in the correlation diagrams of both analyses because of the very low carbon content (~0.1%). Second, reporting the proportion of total events that are multi events does not seem relevant as the number of identified family related to carbon differs between the two analyses (Fig. 4). Indeed, it is very likely that ions from different families do not have the same probability to induce multiple events. Still, assuming that the following dissociation reaction $(C_2)^{2+} \rightarrow C^+ + C^+$ reported in Peng et. al [3] occurred, a higher proportion of multi C+ events should reflect a higher probability of $(C_2)^{2+}$dissociation. 8,15% of C^+ events that are multi-events were reported in the lowest electric field analysis against 17.64% in the highest electric field analysis. This result support the assumption that more molecular ions dissociations related to carbon occurred in the highest electric field analysis.

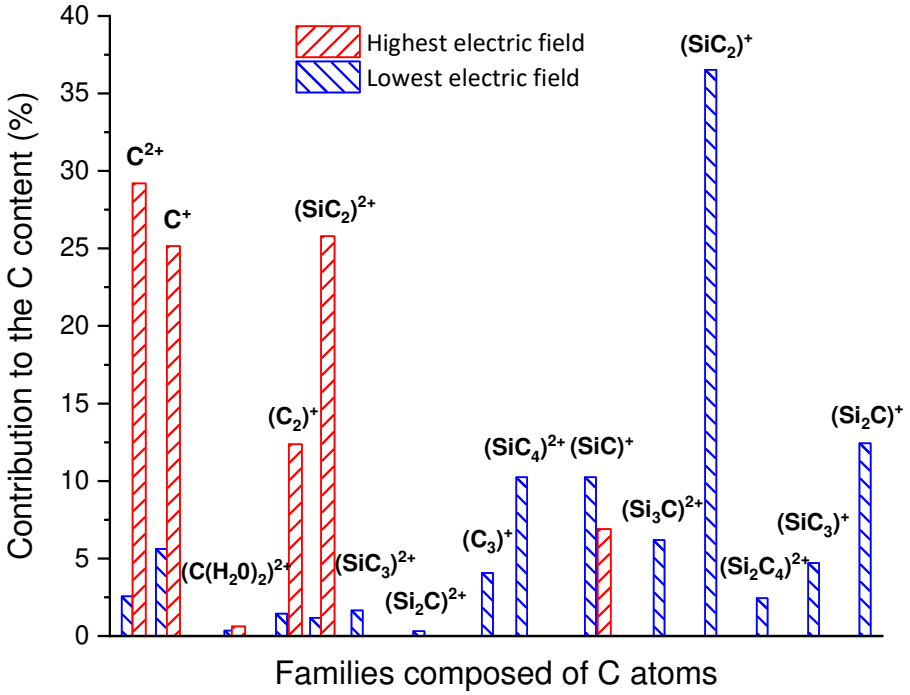

Fig. 4. Histogram of the families respective contribution to the carbon content in both analyses. Contribution are sorted in mass-to-charge ratio increasing order.

APT carbon concentration profiles versus implantation depth were plotted in Fig. 5. SIMS profile has been calibrated from the implanted carbon dose (2 ± 0.02 x 10^{15} ions cm^{-2}). APT concentration profiles were built using sampling slices 1 nm thick and derived from the atomic volume of silicon (0.02 nm^3). The measured SIMS dose integrated over 175 nm is equal to 1.93 x 10^{15} ions cm^{-2} whereas that derived from APT experiments are 1.47 x 10^{15} ions cm^{-2} and 8.51 x 10^{14} ions cm^{-2} for the lowest and highest electric field analysis respectively. Much more accurate quantification is obtained using low electric field conditions. As assumed previously, it is thought that dissociation of unstable molecular ions is promoted at higher electric fields. As a result, because multi-events occur after dissociation, more ions composed of silicon and/or carbon may have been lost in the detection process in the highest electric field analysis [3,7]. The impact of the latter on the silicon content is thought to be negligible because only about 0.4% of silicon ions were detected in the form of molecular ions in both analyses. In contrast, this is not the case for carbon as 45% of its content was detected in the form of molecular ions (Fig. 4).

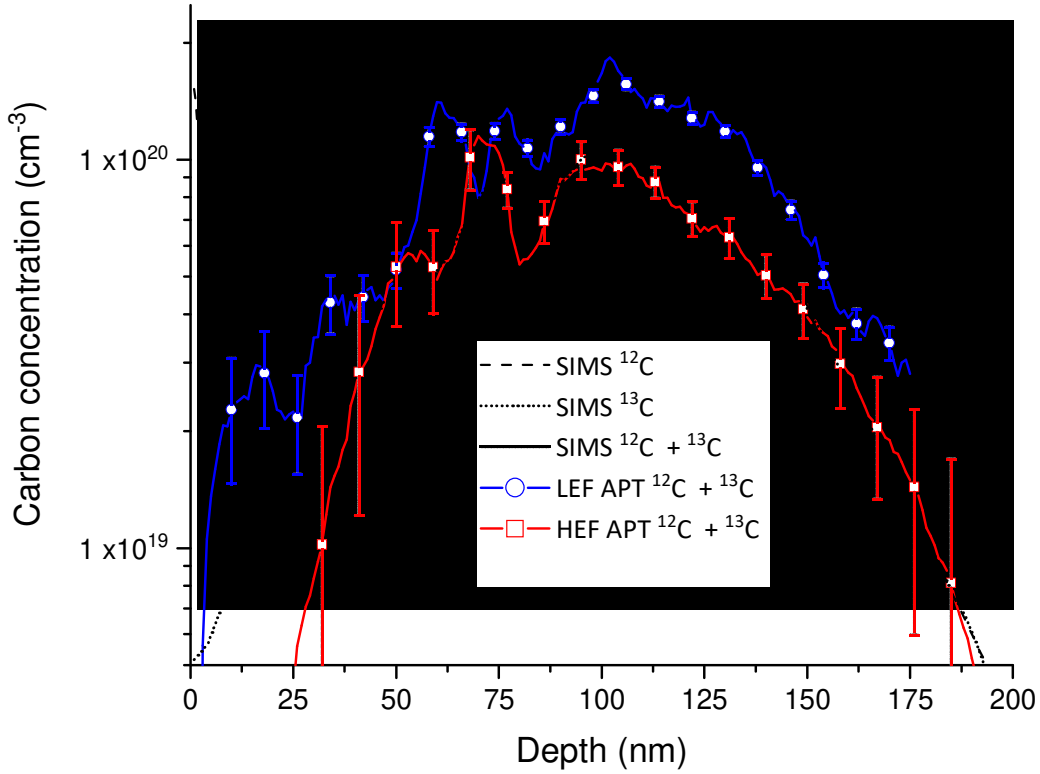

Fig .5. APT and SIMS carbon concentration profiles with implantation depth. Error bars delimits the uncertainty window derived from counting statistics and background subtraction. LEF and HEF respectively stand for Lowest Electric Field and Highest Electric Field.

Another composition-based cluster identification [20] was applied to both analyses in the objective to reveal carbon enriched-clusters below the implantation peak and carbon segregations at structural defects [11,16]. Defects and related carbon segregations are not expected in the first 50 nm as no redistribution in the carbon SIMS profiles is observed (Fig. 5). From these considerations, the composition threshold of the cluster composition was set at 5% so as to exclude carbon ions originating from the first 50 nm. The minimum number of atoms per cluster N_{min} was then determined by observing the reconstructed images for various increasing values of N_{min}. Setting N_{min} at 7 solute atoms was found reasonable so as to avoid tiny fortuitous clusters.

The atom map revealing carbon ions after cluster identification for the lowest electric field analysis is shown in Fig. 6. First, carbon segregations from 50 to 100 nm reveal structural defects that nucleate during recrystallization of a specific type of ion implantation induced amorphous layer [22,11]. The first 50 nm that were excluded from cluster identification corresponds in fact to recrystallized silicon in which carbon lie in solid solution [11,19]. In addition, 90 tiny carbon-enriched clusters of 2 to 3 nm diameters were found below the implantation peak. They precisely grow here because of the supersaturation of self-interstitials that drives carbon diffusion and its precipitation [11]. These clusters are not pure in carbon: they contained silicon atoms which are part of self-interstitials induced by ion implantation [16,17,18]. Self-interstitials are known to drive transient enhanced diffusion of dopants and the maturation of extended defects which are both to inhibit in the design of implanted-doped layers [23,24]. That is why the atomic fraction of carbon in these clusters is of interest for the design of devices as it gives the number of trapped self-interstitials per carbon atom. In other works [16,17], the trapping ratio is found close to one, in agreement with the expected stoichiometry of the SiC phase present in the phase diagram [25]. However, in a recent APT study, the atomic fraction was found well below that of the SiC phase (2.5 at. % against 50 at. %) [11]. This value was obtained from the distribution of distances between 1NN carbon events. As this method disregards the number of carbon atoms in molecular ions, it is now clear that it leads to an underestimation of the carbon amount.

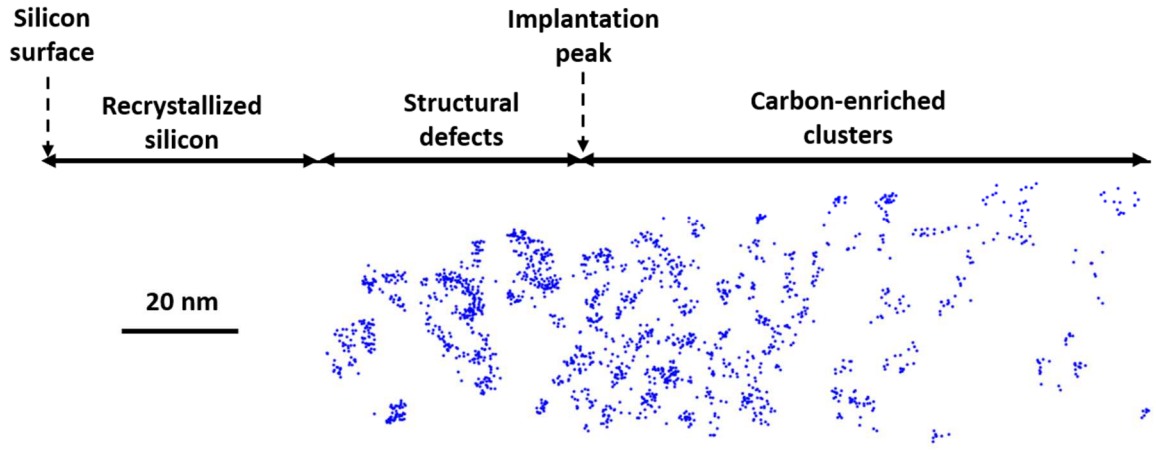

Fig. 6. 3D distribution of carbon ions along the implantation axis after cluster identification (obtained from the lowest electric field analysis). 90 carbon enriched-clusters of average radii 2.5 +/- 0.5 nm were found below the implantation peak. This corresponds to a cluster volume fraction of 0.0046+/- 0.0003.

The average composition of carbon-enriched clusters shown in Fig. 6 was deduced from an erosion profile [26] (Fig. 7). Away from the interface, composition is that of the matrix. The existence of a plateau in both profiles demonstrate that the core of the carbon-enriched zone is not affected by local magnification effects and related trajectory overlaps [27]. This makes it possible to derive a core composition close to 27 at. % at high field and 46 at. % at low field. This clearly show that the atomic fraction of carbon approaches the expected stoichiometry (50 at. %) only in low electric field conditions. This agrees with what was shown for the overall carbon level (Fig. 5).

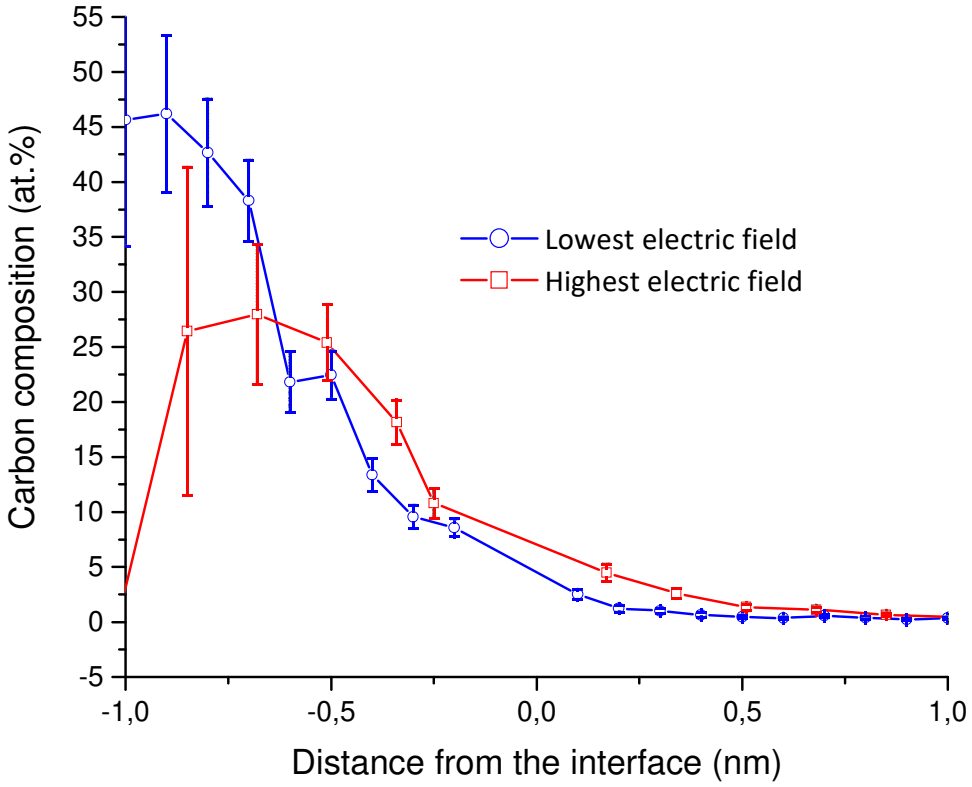

Fig. 7. Erosion profile of the carbon composition in carbon-enriched clusters. Error bars delimits the uncertainty window derived from counting statistics.

4. Conclusion

Atom Probe Tomography was employed to quantify carbon in implanted silicon at two various electric fields (~ 15 and 20 V/nm). Most peaks were related to molecular ions originating from carbon-enriched clusters that nucleate due to carbon supersaturation.

Statistics and equal proportions of implanted ^{12}C and ^{13}C were successfully used to identify peaks and quantify the amount of carbon. Every mass-to-charge overlap was indeed resolved. We now know that $(C_2)^{2+}$ ions are absent for electric fields close to those used in the present

study. $(C_3)^+$ family contribution to the carbon content was derived despite the presence of $((H_2O)_2)^+$ ions.

It has been also shown that molecular ions significantly contribute to the carbon content. The fact that this contribution decreases when the electric field increases was attributed to the promotion of molecular ion dissociations close to the tip surface at higher electric fields. This in turn lead to a much more accurate carbon quantification using low electric fields (less multi-events and consequently less detection biases).

Finally, the atomic fraction of carbon in clusters was derived from the value of the plateau in erosion profiles and was found close to that of the expected SiC phase when using low electric field conditions (high laser power).

Acknowledgment:

The authors thank the STMicrolectronics Crolles Thermal Treatment Team for the design of a relevant annealing inducing carbon clustering and F.Verpilllot for the helpful discussions regarding molecular ion dissociation.

[1] Thuvander, Mattias, et al. "Quantitative atom probe analysis of carbides." Ultramicroscopy 111.6 (2011): 604-608.

[2] Estivill, Robert, et al. "Quantitative analysis of Si/SiGeC superlattices using atom probe tomography". Ultramicroscopy 159 (2015): 223-231.

[3] Peng, Zirong, et al. "On the detection of multiple events in atom probe tomography." Ultramicroscopy 189 (2018): 54-60.

[4] Yao, L., et al. "On the multiplicity of field evaporation events in atom probe: A new dimension to the analysis of mass spectra." Philosophical Magazine Letters 90.2 (2010): 121-129.

[5] Jagutzki, Ottmar, et al. "Multiple hit readout of a microchannel plate detector with a three-layer delay-line anode." IEEE Transactions on Nuclear Science 49.5 (2002): 2477-2483.

[6] Meisenkothen, Frederick, et al. "Effects of detector dead-time on quantitative analyses involving boron and multi-hit detection events in atom probe tomography." Ultramicroscopy 159 (2015): 101-111.

[7] Peng, Zirong, et al. "Unraveling the Metastability of C n 2+(n= 2–4) Clusters." The journal of physical chemistry letters 10.3 (2019): 581-588.

[8] London, Andrew J. "Quantifying uncertainty from mass-peak overlaps in atom probe microscopy." *Microscopy and Microanalysis* 25.2 (2019): 378-388.

[9] Martinavičius, Andrius, et al. "Mechanism of Si3N4 precipitation in nitrided Fe-Si alloys: A novel example of particle-stimulated-nucleation." Materials Letters 189 (2017): 25-27.

[10] Lefebvre, Williams, Francois Vurpillot, and Xavier Sauvage, eds. "Atom probe tomography: put theory into practice", pages 150 and 153. Academic Press, 2016.

[11] Dumas et al. "3D atomic-scale investigation of carbon segregation in phosphorus co-implanted silicon." Applied Physics Letters 115.13 (2019): 132103.

[12] Kingham, David R. "The post-ionization of field evaporated ions: A theoretical explanation of multiple charge states." Surface Science 116.2 (1982): 273-301.

[13] Kelly, Thomas F., et al. "Laser pulsing of field evaporation in atom probe tomography." Current Opinion in Solid State and Materials Science 18.2 (20 81-89.

[14] Vella, A., and J. Houard. "Laser-Assisted Field Evaporation." Atom Probe Tomography. Academic Press, 2016. 251-278.

[15] Hatzoglou, Constantinos, et al. "Preferential evaporation in atom probe tomography: an analytical approach." arXiv preprint arXiv:2008.08801 (2020).

[16] Cristiano et al. "Interstitial trapping efficiency of c+ implanted into preamorphised silicon—control of EOR defects." Nuclear Instruments and Methods in Physics Research Section B: Beam Interactions with Materials and Atoms 127 (1997): 22-26.

[17] Cacciato et al. "Dislocation formation and B transient diffusion in C coimplanted Si." Journal of applied physics 79.5 (1996): 2314-2325.

[18] Goesele, Ulrich, et al. "Diffusion engineering by carbon in silicon." MRS Online Proceedings Library Archive 610 (2000).

[19] Strane, J. W., et al. "Carbon incorporation into Si at high concentrations by ion implantation and solid phase epitaxy." Journal of applied physics 79.2 (1996): 637-646.

[20] Marquis, Emmanuelle A., et al. "On the use of density-based algorithms for the analysis of solute clustering in atom probe tomography data." Proceedings of the 18th International Conference on Environmental Degradation of Materials in Nuclear Power Systems–Water Reactors. Springer, Cham, 2019.

[21] Stanley, R. P. Enumerative Combinatorics, Volume I, Cambridge U. Press, Cambridge, 1997.

[22] Jones, Kevin S., S. Prussin, and E. R. Weber. "A systematic analysis of defects in ion-implanted silicon." Applied Physics A 45.1 (1988): 1-34.

[23] Minondo, M., J. Boussey, and G. Kamarinos. "The impact of the substrate preamorphisation on the electrical performances of p+/n silicon junction diodes." Microelectronics Reliability 37.1 (1997): 53-60.

[24] Cowern, Nicholas, and Conor Rafferty. "Enhanced diffusion in silicon processing." Mrs Bulletin 25.6 (2000): 39-44.

[25] Olesinski, R. W., and G. J. Abbaschian. "The C− Si (carbon-silicon) system." Bulletin of alloy phase diagrams 5.5 (1984): 486-489.

[26] Vaumousse, D., A. Cerezo, and P. J. Warren. "A procedure for quantification of precipitate microstructures from three-dimensional atom probe data." Ultramicroscopy 95 (2003): 215-221.

[27] Blavette et al. "A model accounting for spatial overlaps in 3D atom-probe microscopy." Ultramicroscopy 89.1-3 (2001): 145-153.